The evolution process of a prolonged compound drought and hot extreme event in Southwest China during the 2019 pre-monsoon season

Zuo Wen, Rong Yu, Panmao Zhai, Yixing Yin, Laurent Li

A prolonged compound drought and hot extreme event in Southwest China during the 2019 pre-monsoon season

Zuo Wen[1], Rong Yu[2], Panmao Zhai[2], Yixing Yin[3,4*], Laurent Z.X. Li[5]

1. School of Atmospheric Sciences, Nanjing University of Information Science & Technology, Nanjing 210044, China
2. State Key Laboratory of Severe Weather, Chinese Academy of Meteorological Sciences, Beijing, 100081, China
3. School of Hydrology and Water Resources, Nanjing University of Information Science & Technology, Nanjing 210044, China
4. State Key Laboratory of Hydrology-Water Resources and Hydraulic Engineering, Nanjing Hydraulic Research Institute, Nanjing 210029, China
5. Laboratoire de Météorologie Dynamique, CNRS, Sorbonne Université, Ecole Normale Supérieure, Ecole Polytechnique, Paris 75005, France

Abstract

The latest IPCC AR6 pointed out that some weather and climate extremes, such as temperature extremes and droughts have increased in frequency and/or intensity significantly under global warming background. Based on in situ observations, ERA5 hourly reanalysis and CRA-Land surface reanalysis data, this study described the occurrence and evolution process of compound drought and hot extreme event (CDHEE) in Southwest China in the pre-monsoon season (March-June) in 2019. The spatio-temporal evolutions of key physical variables were diagnosed from the perspective of local land-atmosphere interaction. The Liang-Kleeman Information Flow was firstly used to reveal the interactions between the key variables in CDHEE. In order to find the physical processes which may exist in this event, the CDHEE was divided into three development stages based on the soil moisture reduction. Further diagnostic analysis shown that the trigger variable contributing to CDHEE are not consistent in these three stages. At the first stage, CDHEE was induced by extreme high temperature, which promoted the evaporation, leading to the decrease of soil moisture. Meanwhile, increase of sensible heat promoted the rise of temperature further. Consequently, a positive feedback cycle formed and CDHEE intensified. At the second stage, CDHEE was triggered by precipitation deficit, which broke the water budget, thus soil moisture was decreased by evaporation and CDHEE deteriorated further. At the third stage, precipitation deficit and extreme high temperature are both triggers. Combined effects of high temperature and drought lead to stronger land-atmospheric interaction and feedback. Thus, based on this study, it reveals that extreme high temperature and drought had an obvious interact with each other in the whole process, and extreme high temperature not only was an external environment of others variables, but also involved in local processes.

Keywords: extreme high temperature, drought, compound event, Southwest China, land-atmosphere interaction

0.Introduction

Some weather and climate extremes, such as temperature extremes, heavy precipitation and pluvial floods, river floods, droughts, and storms, have increased in the frequency and/or intensity significantly under global warming background (IPCC, 2021). The increasing number of high-impact events suggests that impacts of weather and climate extremes in practice may not be uniquely determined by a single extreme, but may be related to a combination of factors that lead to high impacts. Such events are generally referred to as compound extreme events (Sadegh et al., 2018). The latest IPCC AR6 defined compound events broadly as "the combination of multiple drivers and/or hazards that contributes to societal or environmental impact (IPCC, 2021). Recently, compound drought and hot extreme event (CDHEE) is one of the most typical events, threatening ecological security and human health seriously (Mazdiyasni and AghaKouchak, 2015; Obladen et al., 2021; Vogel et al., 2019; Zscheischler et al., 2018). Studies have shown that the concurrence probability of CDHEEs in many regions of the world has greatly increased (Mukherjee et al., 2022, 2020). In China, some studies have also found that global warming increases the probability of CDHEEs (Chen and Sun, 2017; Chen et al., 2019; Tavakol et al., 2020; Yu and Zhai, 2020a, 2020b). However, mechanism study of the interaction between drought and hot extreme events is a key point to understand the development of the compound events, which is also conducive to attribution and prediction research (Kong et al., 2020).

Located in the junction of tropical and subtropical climate zone, Southwest China (SWC) is a region with the richest

biodiversity and fragile ecology (Li et al., 2003; Wang et al., 2015). Recently, many studies have indicated that the drought events in SWC have increased, especially during pre-monsoon season (Gao et al., 2018; Han et al., 2016). Spring to summer is the hottest period for SWC. It is easy to induce the concurrence of drought and hot extreme events, i.e, CDHEE, when precipitation is severely insufficient. However, what is the physical mechanism of CDHEE in SWC? This issue needs to be addressed to understand and predict CDHEEs.

During pre-monsoon season from spring to summer in 2019, SWC suffered a severe CDHEE. For Yunnan Province, meteorological drought intensified and the proportion of severe and extreme drought areas increased in May. At the same time, hot extreme events set a new record from 1961 to 2019. The drought damaged area and the losses in Yunnan Province were the heaviest in the past five years (http://www.ynsjzwzcbzx.org.cn/100/103/content_797.html;CMA, 2020a; YPMB, 2020). Based on the 2019 extreme case in SWC, this study attempts to address the occurrence of drought events and further explore land-atmospheric interaction in the development processes of CDHEE.

1. Data and methods

1.1 Data

This paper adopted the ERA5 hourly reanalysis dataset from ECMWF, including horizontal wind and specific humidity at multilevel, and the surface data including total precipitation, 2m temperature, sensible heat flux (SSHF) and latent heat flux (SLHF). The horizontal resolution is 0.25° × 0.25°. Then, these data were processed into daily scale. The daily soil moisture (SM) data from the CRA_LAND surface reanalysis dataset was provided by the National Meteorological Information Center of China Meteorological Administration, with horizontal resolution of 1.0°×1.0°.

In addition, we used the "Dataset of Daily Surface Observation from Chinese Surface Stations (V3.0)", which was provided by the National Meteorological Information Center of China Meteorological Administration (Ren et al., 2012), including daily observed data of precipitation, temperature and relative humidity from 1981 to 2019.

Standardized Soil Moisture Index (SSMI) was used to describe the soil drought (Farahmand and AghaKouchak, 2015). It is consistent with the drought classification of standardized precipitation index (SPI): SSMI≤-0.5 is light drought, SSMI≤-1.0 is moderate drought, SSMI≤-1.5 is severe drought, SSMI≤-2.0 is extreme drought. Here, a drought event was defined when the drought index (SPI/SSMI) reached moderate drought. The hot extreme event was defined when daily maximum temperature was over 90 percentile thresholds (reference period 1981-2019). CDHEEs were defined as the concurrence of drought events and hot extreme events on a daily-time scale basis.

1.2 Methods

Vapor Pressure Deficit (VPD) was used to describe the atmospheric water demand. The calculation formula is as follows:

$$VPD = 0.61078 \times e^{\frac{17.27 \times T_a}{T_a + 237.3}} \times (1 - RH)$$

Where T_a is the average temperature, RH is the relative humidity. The greater value of VPD indicates the greater atmospheric water demand.

Bowen ratio was used to express how available energy at the surface is partitioned, which is defined as the ratio of sensible heat flux to latent heat flux:

$$\beta = \frac{SH}{LH}$$

Where LH is surface latent heat flux, and SH is surface sensible heat flux. When the values of β approach 1, sensible heat and latent heat play the same role in heating the atmosphere; when the value is large than 1, sensible heat plays a leading role in heating the atmosphere; when the value is less than 1, the latent heat flux plays a leading role and transfers energy to the atmosphere in the form of evaporation.

The Liang-Kleeman Information Flow method was used to explore the possible land-atmosphere interaction processes among the variables in this CDHEE. The calculation method of information flow is as follows:

Given the time series X_1 and X_2, Liang (2014) proved that the maximum likelihood estimate of the information flow

from X_2 to X_1 is:

$$T_{2\to1} = \frac{C_{11}C_{12}C_{2,d1} - C_{12}^2 C_{1,d1}}{C_{11}^2 C_{22} - C_{11}C_{12}^2}$$

Where C_{ij} is the covariance of X_i and X_j, and $C_{i,dj}$ is the covariance of the new sequence formed by the forward difference of X_i and X_j. If $|T_{2\to1}| \neq 0$ and passes the 90% confidence test, then X_2 is a cause of X_1 (or X_1 is a consequence of X_2), and otherwise, it is not.

While discussing the interaction between the variables and SM in continuous time, a 14-day-window (6 days before and 7 days after a certain day) was selected based on duration of the different stages, and the triggers of different stages were judged by the 1-day-lead correlation coefficients calculated based on running windows between the variables.

2.Result

2.1 Occurrence of 2019 drought and hot extreme events

Precipitation in SWC is strongly influenced by the Indian monsoon, East Asian summer monsoon and the westerlies. About more than half of precipitation in SWC comes from Indian monsoon, and the westerlies play the second role in water vapor supplies (Zhang, 2020). As can be seen from Fig. 1*a*, the precipitation deficit from March to mid-May in 2019 was accompanied by weak meridional water vapor flux. Meanwhile, less water vapor was transported to SWC. The atmosphere condition over SWC was dry, which was not favorable for precipitation. However, a strong southwesterly water vapor flux appeared in the west side of SWC (90~96°E) in early May. The westerlies allowed some water vapor to arrive the SWC, which might contribute to the light rainfall in mid-May. According to the Climate Bulletin of China Meteorological Administration in 2019 (CMA, 2020), the rainy season in SWC began in June 10, when the southwesterly water vapor flux was obvious. There was strong meridional water vapor transportation. Also, precipitation increased significantly. In addition, unusual weak southern branch trough played a critical role in the occurrence and persistence of drought in SWC, which might lead to unusually weak water vapor transport (Ding and Gao, 2020).

From April to June in 2019, SWC, Myanmar and Laos experienced precipitation deficit and long duration of hot extreme events (Fig. 1*b*). Precipitation was the lowest during the period from 1961 to 2019 in SWC, where the precipitation deficit is more serious than that in surrounding areas. The total number of hot extreme days in SWC exceeded 30 days. Both precipitation deficit and extreme high temperature exacerbated the drought development. Hot extreme event and drought concurred in the same area, which induced rapid development of CDHEEs. The total number of days and evolution of affected areas of CDHEEs are shown in Fig. 2.

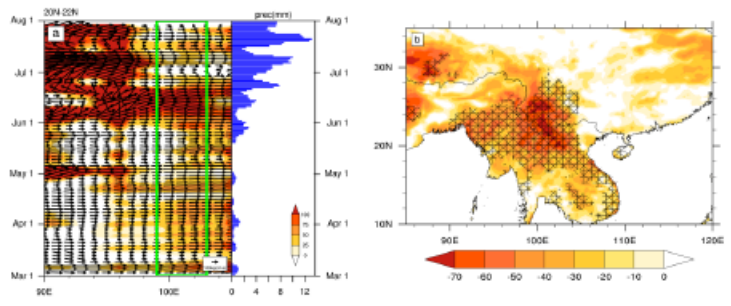

Fig. 1 (a) Transport of water vapor flux (vertical integral to 300hPa) and evolution of regional average precipitation over SWC from March to July in 2019 (shadow: meridional water vapor flux, unit: kg(m · s)$^{-1}$; vector: resultant vapor flux, unit: kg (m · s)$^{-1}$; Blue bar: regional average precipitation, unit: mm). (b) Percentage distribution of precipitation anomaly (shadow, relative to 1981-2010), and regions with accumulated high temperature days over 30 days in Southwest China and Southeast Asia from April to June in 2019 (grid).

The results show that the days of CDHEE was far more numerous and concentrated in SWC, the maximum number of cumulative days was up to 35 days. Therefore, SWC (red box in Fig.2, 98~103°E, 22~28°N) was selected as the study area to explore how the event intensified locally in SWC during the development of CDHEE, and how hot extreme event and drought interacted with each other. As can be seen from the time evolution of the disaster area of CDHEE in SWC, it increased from March and expanded rapidly in early April, reaching the maximum of $21\times10^4 km^2$ on May 19, and then reduced rapidly.

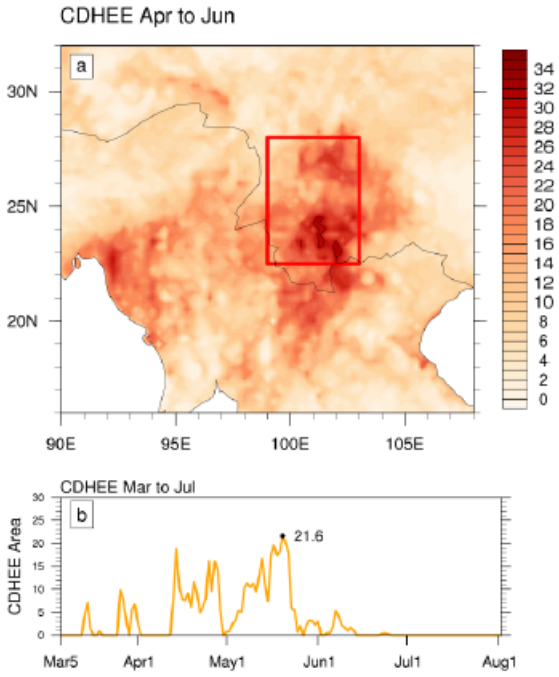

Fig. 2 (a) Spatial distribution of cumulative occurrence days of CDHEE from April to June, and (b) evolution of damaged area (unit: 10^4 km^2) in Southwest China from March to July 2019.

In general, the anomalous water vapor transportation resulted in the delayed rainy season in SWC. With persistent rainfall deficit, the soil tended to dry out. At that time, SWC gradually changed from cold to warm, and the temperature continued rising to the warmest period. A CDHEE thus occurred in SWC during the 2019 pre-monsoon season.

2.2 Evolution of CDHEE processes

Considering that it takes soil moisture (SM) at different depths different time to respond to drought, and the intensity of land-atmosphere interaction is also different, SM at a depth of 10cm from the surface was selected to reflect its dynamic situation (Souza et al., 2021). As shown in Fig. 3*a*, the SSMI reached the level of light drought as early as March, and then intensified to near moderate drought. In April, the drought developed from moderate to severe drought. In May, the drought exacerbated. It was near the extreme drought level in late May, when the drought reached its peak and then eased rapidly. Due to the arrival of rainy season, the precipitation increased persistently, which relieved the SM shortage quickly and made the SSMI rise rapidly. It is worth noting that for the entire March-June, there were three rapid declines of SSMI, corresponding

to the three intensified processes of soil drought. Based on these three declines of SSMI, we divided this event into three development stages. The first stag (stage I) is from March 10th to March 30th, the second stage (stage II) is from April 9th to April 26th, and the third stage (stage III) is from May 5th to May 21th. According to the precipitation changes in Fig. 3*b*, the reason why the CDHEE was divided into three stages is that the process of CDHEE was interrupted by short-term precipitation.

The magnitude of latent heat reflects the energy absorbed by water during evaporation. In this study, the latent heat flux was used to reflect evaporation. Fig. 3*a* shows that the evaporation rate was weak during the compound event and increased after the event ended. The latent heat flux was stable at a low value in March. It suggests that water content which is likely to undergo phase transition was limited, and the SSMI reached drought condition, thus soil evaporation was weak. From the perspective of energy distribution, the Bowen ratio was larger than usual since March, and the anomaly kept increasing and lasted until late June. The largest anomaly was in mid-late May, when the average sensible heat flux in the region was about 6 times of latent heat flux. After that, Bowen ratio began to decline and the abnormal state eased gradually. It can be found that latent heat flux was small and stable during the period (indicating that land surface evaporation was small and stable), and sensible heat flux increased significantly, indicating that land surface energy was mainly transferred to the atmosphere in the form of sensible heat flux. In late May, sensible heat flux began to decrease, latent heat flux began to increase, Bowen ratio also decreased to less than 1 gradually, and latent heat flux became dominant.

In Fig. 3*b*, the evolution of precipitation, temperature and VPD is further analyzed. The data used are all observed in situ data. The results show that the regional average maximum temperature continued to exceed the threshold of 90 percentile from the beginning of March to the end of June, during which the maximum temperature continued to rise. The maximum temperature reached the peak occurred on May 15, then began to decrease. There was an obvious decline process at the end of June, the temperature was below the threshold, and the high temperature process ended. Regional average rainfall was less than usual and the negative anomaly was very evident since March (Fig. 3*c*). Precipitation was continuously less than usual in early April, the negative anomaly gradually increased, and precipitation deficit reached its maximum on May 17. Then, due to the outbreak of Indian monsoon, precipitation increased gradually, and the negative anomaly decreased gradually, and turned into a positive anomaly in early July. VPD was used to reflect the degree of atmospheric water demand in the study area, so as to judge whether the external environment of soil is conducive to evaporation. The regional average VPD appeared higher in the middle and late March than in the usual period, and this situation lasted from April to early July. During this period, the positive anomaly of VPD increased rapidly, and reached the peak of 2.0kPa in May. It showed that the atmosphere was drier from April to May than usual. However, because VPD is also affected by temperature, it is consistent with temperature changes in the context of water shortage (Teuling et al., 2013), and this can be seen in Fig.3*b*. Through the above analysis, it can be found that there is a certain covariability between the changes of air temperature, precipitation and VPD in the occurrence and development of the compound event.

According to Fig. 3*b*, the triggers of land-atmosphere interaction in the three stages can be inferred. During the whole event, the high temperature anomaly persisted and only weakened during the precipitation period; the precipitation anomaly was significant in the second and third stages, especially in the third stage. In the first stage, the precipitation deficit was not obvious since the precipitation occurred in both the current stage and before, while the high temperature anomaly was the most significant among the three stages. Therefore, high temperature was the trigger for SM decline, which further caused land-atmosphere interaction. High temperature promotes the diffusion of water from soil to the atmosphere, it causes the decline of SM continuously, triggers the interaction between land and atmosphere, and develops compound events. In the second stage, although the high temperature continued, it only maintained the state in the previous state, and the precipitation deficit appeared in this stage, so the precipitation deficit was the trigger for the decline of SM in this stage. The precipitation deficit led to the enhancement of soil unsaturated state and the imbalance of water budget, which triggered the land-atmosphere interaction and promotes the development of CDHEE. In the third stage, although the high temperature anomaly weakened, its absolute value was high, and at the same time, the percentage of precipitation anomalies reached the maximum negative value, so both of them are triggers, which together caused the decline of SM. In general, in the three stages, the precipitation deficit and the high temperature triggered the decline of SM, they caused the land-atmosphere interaction. On the basis of the land-atmosphere interaction, it finally led to the development of CDHEE.

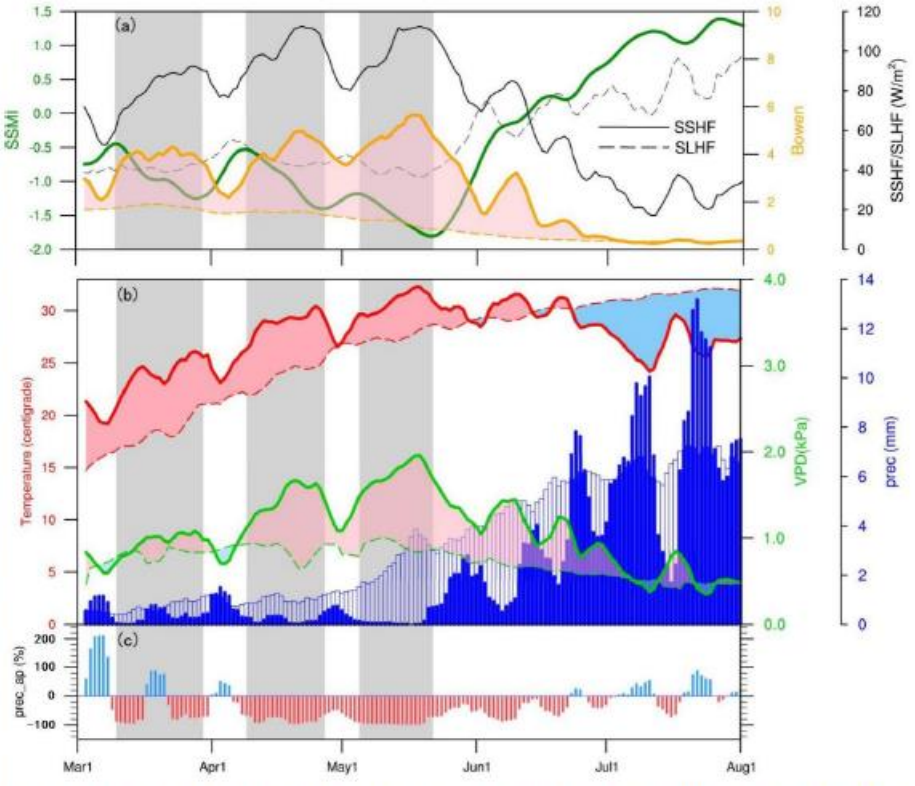

Fig. 3 Temporal evolution of multi-variables from March to July in the study area. (a) Grid variables include surface sensible heat (solid line, J/m²) and latent heat flux (dotted line, units: J/m²), SSMI (green), and Bowen ratio (orange, dotted line shows the climate mean). (b) In situ observation variables include maximum temperature (red, units: ℃, dotted line shows the 90 percentiles threshold), precipitation (blue, units: mm, hollow bar shows the climate mean), VPD (green, units: kPa, dotted line shows the climate mean). The gray shaded areas are the three stages based on the decline of SSMI index. (c) percentage anomaly (red and blue bar chart, units: %).

The frequency of CDHEE, hot extreme event, and SSMI in the three stages is further analyzed, and the results are shown in Fig. 4. As for the frequency distribution, the frequency of CDHEE in the first stage is about 0.1~0.5, and the coverage of CDHEE in the study region is small; the frequency of hot extreme events is also about 0.1~0.5, and the coverage of hot extreme event in the region is also relatively small. The frequency of soil drought is 0.1~0.75, and the coverage is large. Overall, the area and frequency of CDHEE were mainly controlled by hot extreme events. The maximum frequency of CDHEE in the second stage increased to 0.5~0.75, and the area of frequencies between 0.25~0.5 expanded; the frequency of hot extreme events also increased to 0.5~0.75 at this time, and the area of frequencies between 0.25~0.75 expanded to the entire region; the frequency of soil drought increased to 0.75~1.0. Combined with the results of area and frequency, it shows that the frequency of CDHEE is affected by both high temperature and soil drought, but the area is mainly affected by soil drought. In the third stage, the maximum frequencies of CDHEE, hot extreme events and SSMI all reached the values above 0.75. To summarize, the frequency of CDHEE was affected by hot extreme events, and the area was affected by both high

temperature and soil drought.

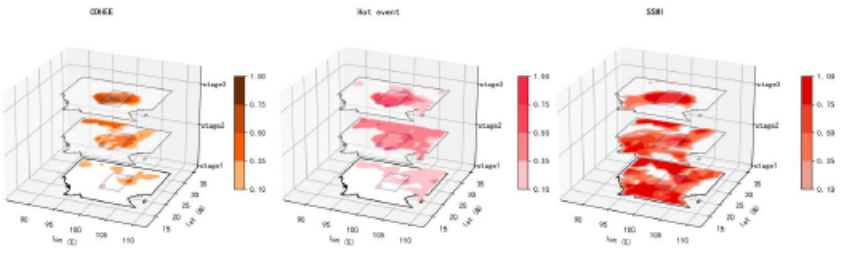

Fig. 4 Frequency distribution of CDHEE, hot extreme event and SSMI at three stages of CDHEE in Southwest China (box) in 2019. only the frequencies above 0.1 were plotted

2.3 Land-atmosphere interactions

In order to further understand the local land-atmosphere interaction process in the CDHEE, on the basis of the above conclusions, this section further uses the correlation analysis and the Liang-Kleeman information flow method to explore the local processes that may occur in the three stages.

It has been obtained above that high temperature and precipitation deficit are the triggers for the development of compound events. Considering that the water retention time in the soil is generally not more than 2 weeks, the lead-lag correlation coefficients of SM with precipitation ($R_{P\text{-}SM}$) and high temperature ($R_{TX\text{-}SM}$) were calculated in a 14-day running window (6 days before and 7 days after a certain day). Considering that SM, precipitation and temperature belong to the cumulative state quantity, flux and instantaneous state quantity, respectively, in the calculation process, the sequence of SM of 1-day forward difference was used; at the same time, the sequence of the difference between the maximum temperature and its 90th percentile threshold was also used, that is, the relationship between the abnormal amount of high temperature and the daily variation of SM was analyzed. It was found that the correlation coefficients between the daily variation of SM and the maximum temperature anomaly/precipitation under the 14-day window were the highest.

As shown in Fig. 5, at the beginning of stage I, the correlation passes the significance test at 0.05 level for $R_{TX\text{-}SM}$, but not for $R_{P\text{-}SM}$. This indicates that the interaction between extreme high temperature and SM was significantly stronger than that between precipitation and SM. Thus, we can infer that extreme high temperature played the main role for CDHEE at stage I. However, all correlation coefficients increased significantly later, indicating that the local land-atmosphere interaction strengthened. Similarly, $R_{P\text{-}SM}$ was significantly stronger than $R_{TX\text{-}SM}$ at the beginning of stage II, suggesting that the land-atmosphere interaction was stimulated by precipitation deficit, which further promoted the development of CDHEE. At stage III, both $R_{TX\text{-}SM}$ and $R_{P\text{-}SM}$ passed the significance test at the beginning, they effect drought together. Because extreme high temperature receded, interaction between extreme high temperature and SM reduce, but precipitation was zero (7 days in 14 days), making it hard to analyze $R_{P\text{-}SM}$ in stage III. Therefore, the triggers of the three stages derived from the lead-lag correlation coefficients are consistent with the previous section.

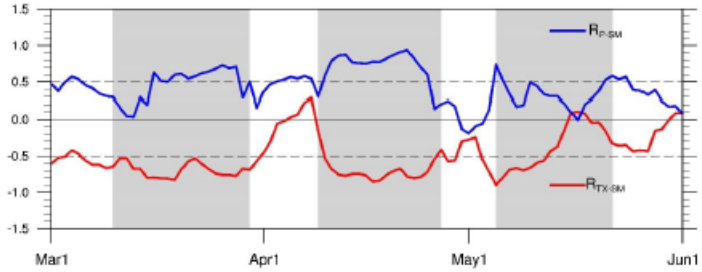

Fig. 5 Running correlation coefficient of precipitation (blue) and extreme high temperature (red) with SM differential in SWC.

Based on the analysis of the physical elements and the results of the running correlation coefficient above, combined with the Liang-Kleeman information flow causal analysis method, the local land-atmosphere interaction relationship in the three stages is analyzed. In the first stage, the information flow results (Tab.1 Stage I) showed that there was a causal relationship between temperature and SM in this stage, and both passed the 99% confidence test. That is, there is a feedback relationship between the two. It is concluded from the above that high temperature was the trigger for SM decline, and the results of information flow further showed that, a feedback relationship developed between the two due to the land-atmosphere interaction after high temperature triggers the decline of SM. The information flow results of the second stage showed (Tab.1 Stage II) that there was a "causal relationship" between SM and precipitation deficit in this stage, and both passed the confidence test of 99%, that is, there was a feedback relationship between the two. The information flow results of the third stage showed (Tab.1 Stage III) that there was a "causal relationship" between SM, precipitation deficit and high temperature in this stage, and they all passed the confidence test of 99%, that is, there were two feedbacks in SM-precipitation and SM-temperature relationships. To sum up, after high temperature and precipitation deficit triggered the decline of SM, they developed feedbacks due to land-atmosphere interactions.

Tab.1 Liang-Kleeman information flow analysis results from three stages

	Stage I			Stage II			Stage III		
	SSMI	Tmax	Prec_a	SSMI	Tmax	Prec_a	SSMI	Tmax	Prec_a
SSMI	-	**0.15**	-	-	-	**0.02**	-	**0.088**	**0.059**
Tmax	**0.713**	-	-	-	-	-	**0.362**	-	-
Prec_a	-	-	-	**0.138**	-	-	**0.1**	-	-

Combining the results of physical elements, cross correlation coefficient, and Liang-Kleeman information flow causal analysis, the local land-atmosphere interaction process at different stages of the CDHEE is presented here. SWC has a special geographical and climatic environment. It is located at the junction of the tropics and subtropics, with sufficient solar radiation and heat. At the same time, dry and wet seasons are very evident, and March-June belongs to pre-monsoon season. During this period, the SM state is conducive to the occurrence and strengthening of land-atmosphere coupling and feedback. Therefore, when the region is controlled by anticyclone, and water vapor transport is negatively anomalous, the abnormal precipitation or temperature will trigger the land-atmosphere feedback, which can easily lead to CDHEE.

The interaction process of the elements in the Stage I can be summarized as follows: The precipitation deficit was not obvious at this time, indicating that the soil water shortage was not large, and evaporation was controlled by solar radiation. Abnormal high temperature promoted soil evaporation (①in Fig. 6), resulting in a decrease in SM. The decreased SM reduced the evaporation, increased sensible heat, and led to the increment of air temperature, which will act on the soil again. This

cycle between the atmosphere and the land promoted the formation of a CDHEE. From the end of March to the beginning of April, a short precipitation process occurred to replenish SM, the temperature dropped, and the CDHEE was alleviated.

The interaction process of elements in the Stage II can be summarized as follows: The precipitation deficit began to intensify(②in Fig. 6) , led to the imbalance of water budget, further drying the soil. The evaporation was limited by SM, and the surface sensible heat increased significantly. At that time, temperature continued to rise, which was conducive to dry the soil, and further increased the temperature. Such a feedback continued, and promoted the development of CDHEE in the second stage. There was precipitation at the end of April, and the compound event eased; but the precipitation was not large, and the SM was still in a dry state, which affected the CDHEE in the third stage.

The interaction process of elements in the Stage III is summarized as follows: The precipitation deficit was the most serious at this time; the temperature also reached the highest; and the strength of land-atmosphere coupling was further strengthened. The possible reason is that, the SM could not be replenished due to the delay of the rainy season, and this was on the basis of the dry soil in the previous stage. But the evaporation continued to consume the water, which increased the dryness of soil and intensified the land-atmosphere coupling. During the process, the temperature continued to rise and the precipitation deficit aggravated (③in Fig. 6), the two above-mentioned triggering mechanisms made the interaction process between the land and the atmosphere intensified, and promoted the development and deterioration of the CDHEE. In late May, the precipitation increased rapidly, replenishing the SM, the temperature dropped, and the CDHEE began to alleviate. With the advent of the rainy season in June, the CDHEE ended.

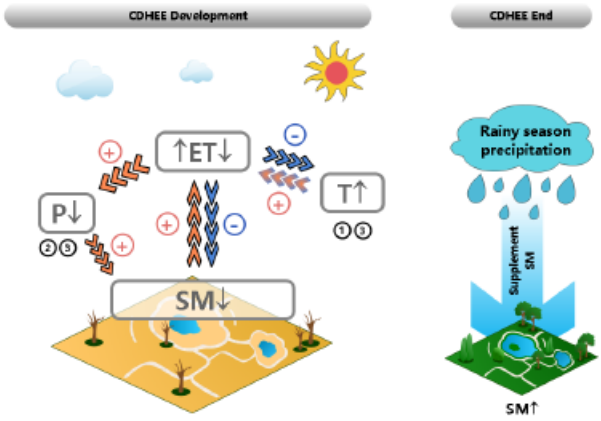

Fig. 6 Process of the three development stages of CDHEE determined by the decline of SSMI index. SM refers to soil moisture; P refers to precipitation; T refers to temperature; ET means evaporation (Orange arrows are positive feedback, blue arrows are negative feedback); ①, ②, ③ refer to Stage I, II and III of CDHEE.

To sum up, this CDHEE was formed through the land-atmosphere interaction mechanism of various positive and negative feedbacks based on the high temperature and precipitation deficit in the early stage. At the same time, we found that this event was first triggered by high temperature, and the impact of high temperature on SM was significant throughout the process. It was not only an element participating in the local process, but also an important influencing factor in the environment.

3.Conclusions

From the perspective of land-atmospheric interaction, this paper discusses the influence of atmospheric and land surface variables on the occurrence and development of the CDHEE in SWC in 2019, reveals the role of each variable in the process.

Related conclusions are as follows:

The pre-monsoon season in 2019 is the most prone to CDHEE. At this time, SWC became warmer gradually, and the temperature kept rising to the warmest period, it was easy to occur hot extreme event. Meanwhile, the unusual weak water vapor transportation resulted in the delayed rainy season in SWC, the soil tended to be dry due to the broken water budget caused by persistent precipitation deficit. They enhanced the feedback mechanism between land and atmosphere, and promoted the occurrence and development of CDHEE.

During the CDHEE from March to June in 2019, the extreme high temperature persisted and only weakened during the occurrence of precipitation; the precipitation deficit was significant in the Stage II & Stage III, especially in the Stage III. In the Stage I, high temperature was the trigger for SM decline, which further caused land-atmosphere interactions. In the Stage II, the precipitation deficit was the trigger for the decline of SM. In the Stage III, both high temperature and precipitation deficit are triggers, they caused SM to decrease. In general, in the three stages, the precipitation deficit and the high temperature triggered the decline of SM, which caused the land-atmosphere interaction, and it finally led to the development of the CDHEE.

The SWC is located at the junction of the tropics and subtropics, and there are sufficient solar radiation and heat, with distinct dry and wet seasons. Pre-monsoon is the transition periods from spring to summer and dry season to wet season. The SM status of relative dryness is conductive to the occurrence and strengthening of land-atmosphere coupling and feedback. Therefore, the reduction of water vapor transport caused by circulation conditions and anomalous anticyclone can lead to abnormal precipitation and temperature, which can trigger the land-atmosphere feedback mechanism and lead to CDHEE easily. The CDHEE in 2019 was formed and developed rapidly through the land-atmosphere feedback mechanism. We found that this event was triggered by the initial extreme high temperature, and the impact of high temperature on SM was significant throughout the process. It was not only an element participating in the local process, but also an important influencing factor in the environment.

There are still many problems that need to be explored in the study of the CDHEE. Firstly, the SM data used in this paper was from shallow soil, but the land-atmosphere interaction may not be limited to the shallow soil, and in order to more accurately reflect the land-atmosphere feedback characteristics, the deeper SM status can be considered. Secondly, soil evaporation is an important process connecting the atmosphere and the land surface. However, soil evaporation is affected by meteorological conditions and SM characteristics. It is difficult to quantitatively describe the actual soil evaporation. This also makes it more difficult to study the land-atmosphere coupling mechanism of CDHEE. Then, due to the limited temporal resolution of the current data such as NDVI and LAI (the highest temporal resolution is once every 8 days), this paper does not consider the impact of vegetation on the CDHEE, but when the temperature is high in the early stage, the vegetation will grow rapidly and absorb a large amount of water from the soil, which will directly promote the formation of the later CDHEE. In addition, vegetation can also indirectly promote the development of CDHEE by affecting precipitation (Li et al., 2018; Zhang et al., 2021).

Author statement

Zuo Wen designed the research, performed the analysis, drafted and revised the manuscript. Rong Yu designed the research, provided comments and revised the manuscript. Panmao Zhai designed the research, provided comments and revised the manuscript. Yixing Yin designed the research, provided comments and revised the manuscript. Laurent Z.X. Li provided comments.

Declaration of competing interest

The authors declare that they have no known competing financial interests or personal relationships that could have appeared to influence the work reported in this paper.

Acknowledgment

This work was jointly supported by the National Key Research and Development Program of China (Grand Number: 2018YFC1507700), the National Natural Science Foundation of China (Grant Number: 41905083), and The Belt and Road

Special Foundation of the State Key Laboratory of Hydrology-Water Resources and Hydraulic Engineering (Grant Number: 2021491311).

Reference

Chen, H., Sun, J., 2017. Anthropogenic warming has caused hot droughts more frequently in China. Journal of Hydrology 544, 306–318. https://doi.org/10.1016/j.jhydrol.2016.11.044

Chen, L., Chen, X., Cheng, L., Zhou, P., Liu, Z., 2019. Compound hot droughts over China: Identification, risk patterns and variations. Atmospheric Research 227, 210–219. https://doi.org/10.1016/j.atmosres.2019.05.009

CMA, 2020. China Climate Bulletin 2019. China Meteorological Administration 20.

Ding, T., Gao, H., 2020. The Record-Breaking Extreme Drought in Yunnan Province, Southwest China during Spring-Early Summer of 2019 and Possible Causes. Journal of Meteorological Research 34, 997–1012. https://doi.org/10.1007/s13351-020-0032-8

Farahmand, A., AghaKouchak, A., 2015. A generalized framework for deriving nonparametric standardized drought indicators. Advances in Water Resources 76, 140–145. https://doi.org/10.1016/j.advwatres.2014.11.012

Gao, C., Chen, H., Sun, S., Ongoma, V., Hua, W., Ma, H., Xu, B., Li, Y., 2018. A potential predictor of multi-season droughts in southwest china: Soil moisture and its memory. Natural Hazards 91, 553–566. https://doi.org/10.1007/s11069-017-3140-8

Han, L., Zhang, Q., Ma, P., Jia, J., Wang, J., 2016. The spatial distribution characteristics of a comprehensive drought risk index in southwestern China and underlying causes. Theoretical and Applied Climatology 124, 517–528. https://doi.org/10.1007/s00704-015-1432-z

IPCC, Seneviratne, S. I., X. Zhang, M. Adnan, W. Badi, C. Dereczynski, A. Di Luca, S. Ghosh, I. Iskandar, J. Kossin, S. Lewis, F. Otto, I. Pinto, M. Satoh, S. M. Vicente-Serrano, M. Wehner, B. Zhou, 2021, Weather and Climate Extreme Events in a Changing Climate. In: Climate Change 2021: The Physical Science Basis. Contribution of Working Group I to the Sixth Assessment Report of the Intergovernmental Panel on Climate Change [Masson-Delmotte, V., P. Zhai, A. Pirani, S. L. Connors, C. Péan, S. Berger, N. Caud, Y. Chen, L. Goldfarb, M. I. Gomis, M. Huang, K. Leitzell, E. Lonnoy, J. B. R. Matthews, T. K. Maycock, T. Waterfield, O. Yelekçi, R. Yu and B. Zhou (eds.)]. Cambridge University Press. In Press. https://doi.org/10.1175/BAMS

Kong, Q., Guerreiro, S.B., Blenkinsop, S., Li, X.F., Fowler, H.J., 2020. Increases in summertime concurrent drought and heatwave in Eastern China. Weather and Climate Extremes 28. https://doi.org/10.1016/j.wace.2019.100242

Li, M., Li, S., Li, Y., 2003. Studies on drought in the past 50 years in China. Chinese Journal of Agrometeorology 24, 7–10. https://doi.org/10.3969/j.issn.1000-6362.2003.01.003

Li, Y., Piao, S., Li, L., Chen, A., Wang, Xu, Ciais, P., Huang, L., Lian, X., Peng, S., Zeng, Z., Li, L.Z.X., Wang, Xuhui, Wang, K., Zhou, L., 2018. Divergent hydrological response to large-scale afforestation and vegetation greening in China. Geophysical Research Letters 10. https://doi.org/10.1126/sciadv.aar4182ï

Liang, X.S., 2014. Unraveling the cause-effect relation between time series. Physical Review E - Statistical, Nonlinear, and Soft Matter Physics 90. https://doi.org/10.1103/PhysRevE.90.052150

Mazdiyasni, O., AghaKouchak, A., 2015. Substantial increase in concurrent droughts and heatwaves in the United States. Proc Natl Acad Sci U S A 112, 11484–11489. https://doi.org/10.1073/pnas.1422945112

Mukherjee, S., Ashfaq, M., Mishra, A.K., 2020. Compound Drought and Heatwaves at a Global Scale: The Role of Natural Climate Variability-Associated Synoptic Patterns and Land-Surface Energy Budget Anomalies. Journal of Geophysical Research: Atmospheres 125. https://doi.org/10.1029/2019JD031943

Mukherjee, S., Mishra, A.K., Ashfaq, M., Kao, S.C., 2022. Relative effect of anthropogenic warming and natural climate variability to changes in Compound drought and heatwaves. Journal of Hydrology 605. https://doi.org/10.1016/j.jhydrol.2021.127396

Obladen, N., Dechering, P., Skiadaresis, G., Tegel, W., Keßler, J., Höllerl, S., Kaps, S., Hertel, M., Dulamsuren, C., Seifert, T., Hirsch, M., Seim, A., 2021. Tree mortality of European beech and Norway spruce induced by 2018-2019 hot droughts in central Germany. Agricultural and Forest Meteorology 307. https://doi.org/10.1016/j.agrformet.2021.108482

Ren, Z., Yu, Y., Zou, F.X., Xu, Y., 2012. Quality Detection of Surface Historical Basic Meteorological Data. Journal of Applied Meteorological Science 23, 739–747. https://doi.org/10.3969/j.issn.1001-7313.2012.06.011

Sadegh, M., Moftakhari, H., Gupta, H. v., Ragno, E., Mazdiyasni, O., Sanders, B., Matthew, R., AghaKouchak, A., 2018. Multihazard Scenarios for Analysis of Compound Extreme Events. Geophysical Research Letters 45, 5470–5480. https://doi.org/10.1029/2018GL077317

Souza, A.G.S.S., Ribeiro Neto, A., Souza, L.L. de, 2021. Soil moisture-based index for agricultural drought assessment: SMADI application in Pernambuco State-Brazil. Remote Sensing of Environment 252. https://doi.org/10.1016/j.rse.2020.112124

Tavakol, A., Rahmani, V., Harrington, J., 2020. Evaluation of hot temperature extremes and heat waves in the Mississippi River Basin. Atmospheric Research 239. https://doi.org/10.1016/j.atmosres.2020.104907

Teuling, A.J., van Loon, A.F., Seneviratne, S.I., Lehner, I., Aubinet, M., Heinesch, B., Bernhofer, C., Grünwald, T., Prasse, H., Spank, U., 2013. Evapotranspiration amplifies European summer drought. Geophysical Research Letters 40, 2071–2075. https://doi.org/10.1002/grl.50495

Vogel, M.M., Zscheischler, J., Wartenburger, R., Dee, D., Seneviratne, S.I., 2019. Concurrent 2018 Hot Extremes Across Northern Hemisphere Due to Human-Induced Climate Change. Earth's Future 7, 692–703. https://doi.org/10.1029/2019EF001189

Wang, L., Chen, W., Zhou, W., Huang, G., 2015. Drought in Southwest China: A Review. Atmospheric and Oceanic Science Letters 8, 339–344. https://doi.org/10.3878/AOSL20150043

YPMB, 2020. Climate Bulletin of Yunnan in 2019. Yunnan Provincial Meteorological Bureau 14.

Yu, R., Zhai, P., 2020a. Changes in compound drought and hot extreme events in summer over populated eastern China. Weather and Climate Extremes 30. https://doi.org/10.1016/j.wace.2020.100295

Yu, R., Zhai, P., 2020b. More frequent and widespread persistent compound drought and heat event observed in China. Scientific Reports 10. https://doi.org/10.1038/s41598-020-71312-3

Zhang, C., 2020. Moisture sources for precipitation in Southwest China in summer and the changes during the extreme droughts of 2006 and 2011. Journal of Hydrology 591. https://doi.org/10.1016/j.jhydrol.2020.125333

Zhang, Y., Keenan, T.F., Zhou, S., 2021. Exacerbated drought impacts on global ecosystems due to structural overshoot. Nature Ecology and Evolution 5, 1490–1498. https://doi.org/10.1038/s41559-021-01551-8

Zscheischler, J., Westra, S., van den Hurk, B.J.J.M., Seneviratne, S.I., Ward, P.J., Pitman, A., Aghakouchak, A., Bresch, D.N., Leonard, M., Wahl, T., Zhang, X., 2018. Future climate risk from compound events. Nature Climate Change. https://doi.org/10.1038/s41558-018-0156-3